Physics in Medicine & Biology

IPEM Institute of Physics and Engineering in Medicine

ACCEPTED MANUSCRIPT

^{4}He dose- and track-averaged linear energy transfer: Monte Carlo algorithms and experimental verification

To cite this article before publication: Serena Fattori *et al* 2022 *Phys. Med. Biol.* in press https://doi.org/10.1088/1361-6560/ac776f

^{4}He dose- and track-averaged Linear Energy Transfer: Monte Carlo algorithms and experimental verification

S. Fattori[1], G. Petringa[1,2,*], S. Agosteo[3,4], D. Bortot[3,4], V. Conte [5], G. Cuttone[1], A. Di Fini[6], F. Farrokhi[7], D. Mazzucconi[3,4], L. Pandola[1], I. Petrović[8], A. Ristić-Fira[8], A. Rosenfeld[9], U. Weber[10] and G.A.P. Cirrone [1,11]

[1]Istituto Nazionale di Fisica Nucleare INFN - Laboratori Nazionali del Sud, Catania, Italy

[2]Extreme Light Infrastructure (ELI)-Beamlines Center, Institute of Physics (FZU), Czech Academy of Sciences, Prague, Czechia

[3]Politecnico di Milano, Dipartimento di Energia, Milano, Italy

[4]Istituto Nazionale di Fisica Nucleare INFN - Sezione di Milano, Milano, Italy

[5]Istituto Nazionale di Fisica Nucleare INFN - Laboratori Nazionali di Legnaro, Legnaro, Italy

[6]Università degli Studi di Catania, Dipartimento di Fisica e Astronomia, Catania, Italy

[7]University of Isfahan, Physic department of university of Isfahan, Iran

[8]Vinča Institute of Nuclear Sciences, University of Belgrade, Belgrade, Serbia

[9]Centre for Medical Radiation Physics, University of Wollongong, Wollongong, Australia

[10]GSI Helmholtzzentrum für Schwerionenforschung GmbH, Biophysics division, Darmstadt, Germany

[11]Centro Siciliano di Fisica Nucleare e Struttura della Materia, Catania, Italy

E-mail: giada.petringa@lns.infn.it

* Corresponding author

May 5, 2022

Abstract.

Objective In the present hadrontherapy scenario, there is a growing interest in exploring

the capabilities of different ion species other than protons and carbons. The possibility of using different ions paves the way for new radiotherapy approaches, such as the multi-ions treatment, where radiation could vary according to target volume, shape, depth and histologic characteristics of the tumor. For these reasons, in this paper, the study and understanding of biological-relevant quantities was extended for the case of ^{4}He ion.

Approach Geant4 Monte Carlo based algorithms for dose- and track-averaged LET (Linear Energy Transfer) calculations, were validated for ^{4}He ions and for the case of a mixed field characterised by the presence of secondary ions from both target and projectile fragmentation. The simulated dose and track averaged LETs were compared with the corresponding dose and frequency mean values of the lineal energy, $\bar{y}_D$ and $\bar{y}_F$, derived from experimental microdosimetric spectra. Two microdosimetric experimental campaigns were carried out at the Italian eye proton therapy facility of the Laboratori Nazionali del Sud of Istituto Nazionale di Fisica Nucleare (INFN-LNS, Catania, I) using two different microdosimeters: the MicroPlus probe and the nano-TEPC (Tissue Equivalent Proportional Counter).

Main results A good agreement of $\bar{L}_d^{Total}$ and $\bar{L}_t^{Total}$ with $\bar{y}_D$ and $\bar{y}_T$ experimentally measured with both microdosimetric detectors MicroPlus and nano-TEPC in two configurations: full energy and modulated ^{4}He ion beam, was found.

Significance The results of this study certify the use of a very effective tool for the precise calculation of LET, given by a Monte Carlo approach which has the advantage of allowing detailed simulation and tracking of nuclear interactions, even in complex clinical scenarios.

Keywords: Linear Energy Transfer, Monte Carlo, Protontherapy, Microdosimetry, Secondary, Target Fragmentation

Submitted to: *Phys. Med. Biol.*

1. Introduction

Clinical hadrontherapy is, nowadays, based on the use of energetic protons (up to 250 MeV) and Carbon (up to 450 AMeV) beams. On the other hand, several groups have recently investigated the opportunity of a combined use of different ions including the Carbon itself

(Tsujii & Kamada 2012, Tessonnier *et al.* 2017, Malouff *et al.* 2020, Lee *et al.* 2021), Helium (Krämer *et al.* 2020, Tessonnier *et al.* 2017, Lee *et al.* 2021), Oxygen (Kurz *et al.* 2012, Sokol *et al.* 2017, Tessonnier *et al.* 2017, Lee *et al.* 2021), and Neon (Lee *et al.* 2021) as therapeutic beams. Tsujii & Kamada (2012) in 2012 presented a review on clinical results of carbon-ion radiotherapy, as well as Malouff *et al.* (2020) in 2020. Tessonnier *et al.* (2017) studied the basic dosimetric features of helium, carbon and oxygen ion beams, for the whole therapeutic energy range. In 2012 Kurz *et al.* (2012) presented the first experimental-based characterization of oxygen ion beam depth dose distributions at the HIT (Heidelberg Ion-Beam Therapy Center). Krämer *et al.* (2020) proposed and validated a model for therapeutic ^{4}He beams based on TRiP98 Treatment Planning System (TPS). Carante (Carante *et al.* 2018) presented an upgraded version of the BIANCA II biophysical model, now also able to well reproduce the damage of proton, carbon and helium beams in terms of survival curves and chromosomal aberrations over a wide LET interval (0.6-502 keV μm$^{-}1$). Sokol *et al.* (2017) reported in 2017 on the experimental verification of biologically optimized treatment plans generated with the TRiP98 planning system with ^{16}O beams. Among the potential interesting candidates for realizing an ion therapy plan there is Helium (^{4}He). Although not yet commonly used in current clinical practice, ^{4}He has already shown encouraging results in the clinical trials realized at the Lawrence Berkeley National Laboratory (LBNL) between 1977 and 1993, with over 2000 patients successfully treated (Mein *et al.* 2019, Ebner *et al.* 2017). After these promising results at the LBNL, ^{4}He therapy remained clinically unexploited, until it was brought to the fore again through the ongoing clinical translation studies at the Heidelberg Ion-Beam Therapy (HIT) Center (Mein *et al.* 2019, Ebner *et al.* 2017). These preclinical studies (Norbury *et al.* 2020, Tessonnier *et al.* 2021, Mairani *et al.* 2021) led, in July 2021, to the first clinical application of helium beams since the time of the LBNL clinical trial, and the HIT center will shortly initiate a larger-scale clinical application campaign. In

the above-depicted scenario and considering its potential clinical implications, it results of undisputed importance extending the understanding of the biological-relevant quantities also for the case of ^{4}He. Among them, we focus on the concept of averaged LET, which consists of the mean value of the restricted stopping power when all particles traversing a given volume immersed in a radiation field are considered. Two main implementations of averaged-LET are nowadays considered: the track-averaged ($\bar{L}_t$) and the dose-averaged ($\bar{L}_d$) LET, the first one based on the using of particles fluence and the second one based on the locally deposited dose, to weigh the electronic stopping power of the beam in a given point of the radiation field. It is well consolidated that $\bar{L}_t$ and $\bar{L}_d$ represent two physical quantities that can be used to describe the biological effectiveness of ion beams (Hawkins 2003, Sørensen *et al.* 2011, McNamara *et al.* 2015, Tommasino & Durante 2015, Mein *et al.* 2019, Friedrich *et al.* 2017, Kalholm *et al.* 2021). $\bar{L}_t$ and $\bar{L}_d$ definitions can be then extended introducing the concepts of track-averaged total ($\bar{L}_t^{Total}$) and dose-averaged total ($\bar{L}_d^{Total}$) LET able to include the contribution of all secondary ions generated in hadronic inelastic interactions, also initiated by the produced secondary neutrons (Wilkens & Oelfke 2003, Romano *et al.* 2014, Petringa *et al.* 2020). The evaluation of $\bar{L}_t^{Total}$ and $\bar{L}_d^{Total}$ can be efficiently realized through Monte Carlo simulations. The introduction and the verification of Monte Carlo based algorithms for the $\bar{L}_t^{Total}$ and $\bar{L}_d^{Total}$ evaluation was already carried out by many authors for clinical proton beams (Romano *et al.* 2014, Cortes-Giraldo & Carabe 2015, Bertolet *et al.* 2019, Petringa *et al.* 2020). In 2014 Romano *et al.* (2014) implemented the $\bar{L}_d$ and $\bar{L}_d^{Total}$ algorithms with the Geant4 Monte Carlo simulation toolkit (Agostinelli *et al.* 2003, Allison *et al.* 2006, Allison *et al.* 2016). Cortes-Giraldo & Carabe (2015) compared unrestricted $\bar{L}_d$ maps, calculated using three different Monte Carlo scoring methods, with dose average LET estimations from microdosimetry calculations. In 2020 Petringa *et al.* (2020) validated Geant4 Monte Carlo (Agostinelli *et al.* 2003, Allison *et al.* 2006, Allison *et al.* 2016) based algorithms for the evaluation of

$\bar{L}_t^{Total}$ and $\bar{L}_d^{Total}$ for the case of clinical proton beams.

In this work the capabilities of Geant4 Monte Carlo toolkit (Agostinelli *et al.* 2003, Allison *et al.* 2006, Allison *et al.* 2016) were coupled with the above mentioned approaches, to calculate the averaged total LETs for the ^{4}He ions case. The simulation results were compared with experimental measurements performed at the Italian ocular proton therapy facility (INFN-LNS, Catania, Italy) (Cirrone *et al.* 2017), using two microdosimeters: the MicroPlus probe (Rosenfeld 2016, Anderson & other 2017) and the nano-TEPC (Tissue Equivalent Proportional Counter) (Bortot *et al.* 2017).

The proposed computational approaches, the experimental set-up, and the description of the two microdosimeters are reported in Section 2 of this paper. In Section 3 the comparisons of the simulation results with the experimental data is reported, as well as a discussion on the role of secondary ions with their specific LET contribution, attempting some considerations to the consequent RBE values expected. In Section 4 we conclude with a general discussion.

2. Materials and methods

2.1. Monte Carlo based LET calculation algorithms and their corresponding experimental quantities

The LET estimation for the ^{4}He was performed using a set of algorithms already proposed by Petringa *et al.* (2020) and entirely tested with clinical proton beam. Since these algorithms do not depend on the mass and the atomic number of the incident particle, they are susceptible to being extended for heavier ions. Petringa *et al.* (2020) report the definition of four different averaged-LET: the total track-averaged LET ($\bar{L}_t^{Total}$), the total dose-averaged LET ($\bar{L}_t^{Total}$), the primary track-averaged LET ($\bar{L}_t$) and the primary dose-averaged LET ($\bar{L}_d$). The first two definitions include the contribution of the secondary ions, possibly generated in the ion-material hadronic elastic and inelastic interactions. The third and the fourth ones, do not

consider this case and take into account only the primary incident beam for the calculations. Supposing to have a particle traversing a given volume of a certain medium, these four quantities are calculated by adopting a Monte Carlo simulation based on the expressions below reported:

$$\bar{L}_T^{Total} = \frac{\sum_{j=1}^{n}[\sum_{i=1}^{N} L_i l_i]_j}{\sum_{j=1}^{n}[\sum_{i=1}^{N} l_i]_j} \quad (1)$$

$$\bar{L}_d^{Total} = \frac{\sum_{j=1}^{n}[\sum_{i=1}^{N} L_i \varepsilon_i]_j}{\sum_{j=1}^{n}[\sum_{i=1}^{N} \varepsilon_i]_j} \quad (2)$$

$$\bar{L}_T = \frac{\sum_{i=1}^{N} L_i l_i}{\sum_{i=1}^{N} l_i} \quad (3)$$

$$\bar{L}_d = \frac{\sum_{i=1}^{N} L_i \varepsilon_i}{\sum_{i=1}^{N} \varepsilon_i} \quad (4)$$

Here, L_i is the tabulated electronic stopping power at a given energy in the given medium, directly retrieved from Monte Carlo, l and ε are the track length and the energy loss of the particle in the given volume. The index *i* runs over the total number of steps *N* carried out by the particle in the volume considered; the index *j* runs over all the particles travelling in that volume, including the secondary ions. In the simplest case, where secondary ions generated in the hadronic interactions are neglected (Eq.3 and Eq.4), the sum over *j* is not present.

The *track*- and *dose*-averaged LET values, both total and primary, were compared with the experimental frequency-mean lineal energy ($\bar{y}_F$) and dose-mean lineal energy ($\bar{y}_D$), respectively defined in Eq.5 and Eq.6:

$$\bar{y_F} = \int y f(y) dy \quad (5)$$

$$\bar{y_D} = \frac{\int y^2 f(y) dy}{\int y f(y) dy} \quad (6)$$

Where *y* is the lineal energy, defined as the quotient of the energy ε imparted to the mass in a sensitive volume by a single energy deposition event by the mean chord length $< l >$ in that volume (i.e. the mean length of randomly oriented chords in that volume). The quantities

$\bar{y}_F$ and $\bar{y}_D$ represent the expected value of *y* through the probability density *f(y)* and the dose probability density of *y*, *d(y)*, respectively (International Commission on Radiation Units & Measurements 1983). In particular, *f(y)* is the derivative, with respect to *y*, of the probability *F(y)*, that the specific energy is equal to or less than *y*:

$$f(y) = \frac{dF(y)}{dy} \tag{7}$$

For each energy value ε in the microdosimetric spectrum, $dF(y)$ is given by the counts for that energy ε dived by the total number of counts of the whole spectrum.

The relation between the distributions *f(y)* and *d(y)* is:

$$d(y) = \frac{y}{\bar{y_F}} f(y) \tag{8}$$

In this work, the $\bar{y}_F$ and $\bar{y}_D$ values were derived from the analysis of the microdosimetric spectra measured with two different microdosimeters: the MicroPlus probe (Rosenfeld 2016, Anderson & other 2017) and the nano-TEPC (Bortot *et al.* 2017, Mazzucconi *et al.* (a) 2018).

2.2. Geant4 Monte Carlo simulation

To implement the calculation of the averaged-LETs as reported in the equations 1- 4, we realized a Geant4 (Agostinelli *et al.* 2003, Allison *et al.* 2006, Allison *et al.* 2016) Monte Carlo simulation based on `Hadrontherapy` (Cirrone *et al.* 2005, Cirrone *et al.* 2011), an advanced example officially released inside the Geant4 toolkit distribution.

`Hadrontherapy` is an open-source application developed for proton and ion dosimetric and radiobiologic studies. It describes the experimental beamline adopted in all the microdosimetric measurements discussed in this paper. Furthermore, `Hadrontherapy` models a voxelized water box at the end of the beamline. This box reproduces a water tank, conventionally used for dosimetric measurements and radiobiology irradiation experiments. The application allows to divide the tank into slices, orthogonal to the beam direction. Each

of them is a sensitive volume where all physical quantities needed for the LETs calculation can be retrieved.

The characteristics of the primary Helium beam (energy, energy spread, beam spot size, spatial and angular divergence) were fixed on the basis of the experimental pristine Bragg peak acquired with an Advanced *Markus* chamber in water and compared with the corresponding simulated peak.

The primary beam was modelled as an ^{4}He beam with a Gaussian energy distribution, centred at the nominal energy of 62 MeV/n, with a standard deviation of 1‰. The beam spot was assumed to be circular and modelled as a bivariate Gaussian distribution with a standard deviation of 2 mm. We considered a beam angular distribution still gaussian with a standard deviation of 0.028 degrees. The energy of the ^{4}He beam was modulated with the proper modulator filter, according to the specific measurement set-up (see Section 2.3).

The `G4EmStandardPhysics_option4` (Ivanchenko *et al.* 2014) physics list was used to model the electromagnetic interactions. The elastic and inelastic hadronic processes were simulated using the `G4HadronElasticPhysicsHP`, the `G4IonElasticPhysics`, the `G4HadronPhysicsQGSP_BIC_AllHP` and the `G4IonPhysicsPHP` models (*Geant4 Physics List Guide* 2020, *Geant4 Physics Reference Manual* 2020). As discussed in Petringa *et al.* (2020) the LET distribution curves calculated with the `Hadrontherapy` application show a negligible dependence on the values of the production cut, i.e., the threshold distance below which secondary particles are not generated and tracked individually (Petringa *et al.* 2020). For this reason, the production cut in this work was fixed to 0.1 mm for electrons, gammas and secondary protons. All simulations were carried out using the `10.06.p02` (May 29th, 2020) Geant4 version. Each simulation run consisted of 1×10^7 primary histories.

2.3. The experimental measurements

2.3.1. Experimental set-up

The experimental microdosimetric measurements were performed in the multidisciplinary beamline of the INFN-LNS laboratory, shown in Figure 1. The 62 AMeV ^{4}He beam, accelerated by a superconducting cyclotron, traversed a 15 μm tantalum foil and exited in the air throughout a 50 μm Kapton window. It then reached the energy modulation system, properly designed to produce a spread out dose profile at the irradiation point. Two energy modulation systems (a "Ridge" and "Ripple" filter) were adopted to create a proper beam energy modulation (Bourhaleb *et al.* 2017, Romano *et al.* 2014, Weber & Kraft 1999).

After the modulation, the beam traversed a monitor chamber for real-time fluence measurements, and a 60 cm long brass final collimator, fixing the ultimate beam emittance at the irradiation point. Finally, the ^{4}He beam reached the microdosimeter, positioned at different depths along the Bragg peak thanks to PolyMethyl Methacrylate (PMMA) slabs of different thicknesses. The ^{4}He beam, at the detector position, had a circular aperture of 25 mm in diameter and a flat dose distribution with an homogeneity better than 5% over 24 mm. The detectors, whose transversal maximum dimensions were less than 10 mm, were positioned, at the beam center with a precision of the order of 100 μm, in the flat fluence section of the particles distribution,

2.3.2. The micro-dosimeters

To obtain the microdosimetric quantities described in Section 2.1, the random distribution of the energy imparted ε by single events was measured for a large number of events. In this work the lineal energy was determined as the quotient of ε by the mean path length $< l_{Path} >$ of the primary charged particles traversing the sensitive volume following the procedure described in Bolst *et al.* (2017).

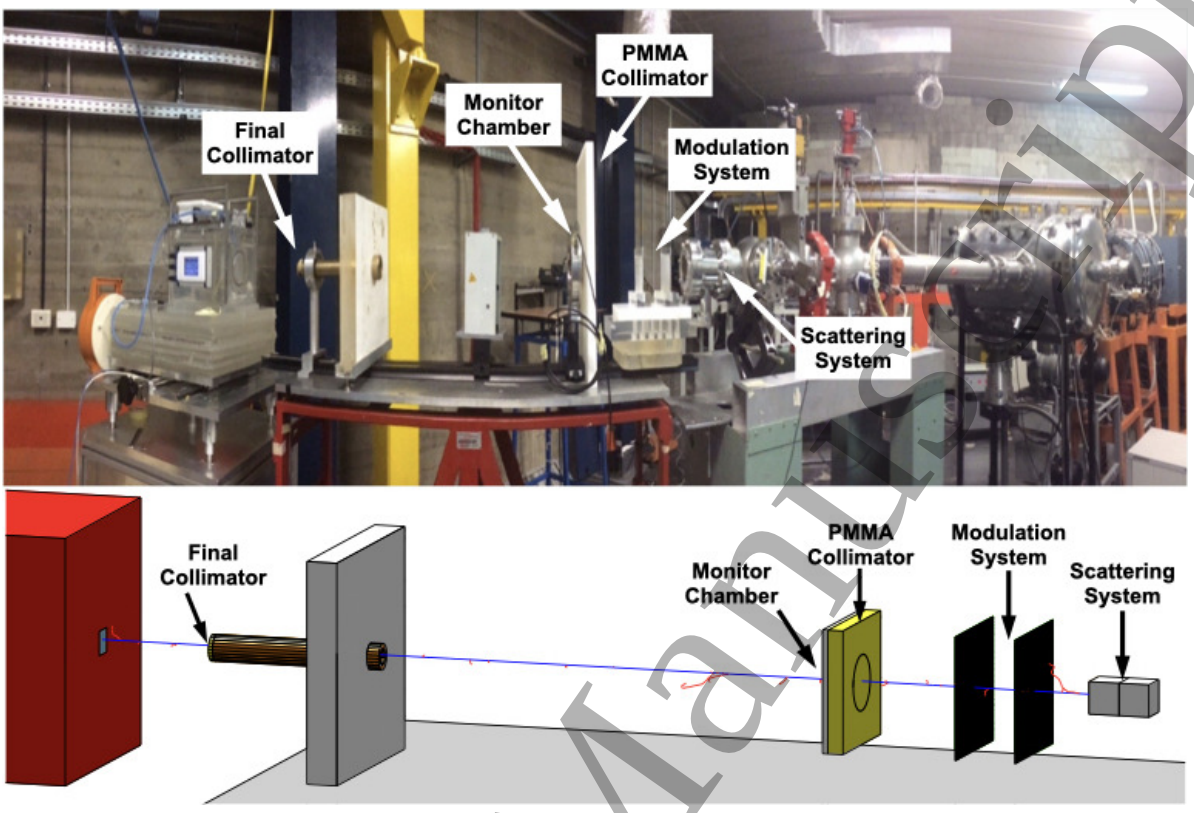

Figure 1. The 0^o beamline at INFN-LNS, from the first scattering foil made of 15 μm tantalum foil, till the water phantom, passing through the modulation system, the collimators, and the monitor chambers. In the image on top, we see a photo of this beamline, while at the bottom, we have its Monte Carlo graphical output.

The two microdosimeters used for the experimental measurements are the MicroPlus probe, developed by the Centre for Medical Radiation Physics of Wollongong University (Wollongong, Australia) (Rosenfeld 2016, Anderson & other 2017), and the nano-TEPC, constructed at the Laboratori Nazionali di Legnaro of Istituto Nazionale di Fisica Nucleare (Legnaro, Italy) (Bortot *et al.* 2017).

The MicroPlus probe is an array of 3D right parallelepiped shape sensitive volumes (diodes) with area $30\mu m \times 30\mu m$, fabricated using silicon on insulator wafers with an active layer of 10 μm thickness. Considering the irradiation geometry, the mean path length of primary particles was considered equal to the thickness of the active layer, i.e. ten micrometres in silicon. The corresponding water-equivalent length was determined with Monte Carlo, obtaining $(17.0 \pm 0.5)\mu m$.

The nano-TEPC is a low-pressure, avalanche-confinement TEPC capable of simulating tissue-equivalent sites down to the nanometer region. The sensitive volume of the microdosimeter is cylindrical (13 mm in diameter and length) and contains three electrodes biased independently: a central graphite anode wire (1 mm in diameter), a tissue-equivalent plastic cylindrical cathode shell (A-150 type, 13 mm in internal diameter, and 1 mm in thickness) and a helix (gold-plated tungsten wire, 100 μm in diameter), 6 mm in diameter. Also for this microdosimeter it was necessary to replace $< l >$ with $< l_{Path} >$. A complete discussion on the chord-length probability distribution for the nano-TEPC is reported in Mazzucconi *et al.*(b) (2018), together with the evaluation of the mean path length for this microdosimeter, which corresponds to $(306 \pm 1)nm$.

Three configurations were adopted for the microdosimetric spectra acquisitions:

- Configuration A: Pristine peak with the MicroPlus probe;
- Configuration B: Modulated peak (with ridge filter) with MicroPlus probe;
- Configuration C: Modulated peak (with ripple filter) with nano-TEPC.

3. Results and Analysis

3.1. Monte Carlo results against experimental microdosimetric data

The experimental campaign was carried out by collecting twelve, eight, and four microdosimetric spectra in configurations A, B, and C, respectively. Depth dose distributions in water were measured with a Markus ionisation chamber (mod.3002, PTW). The penetration range in water, measured as the depth in the distal part corresponding to 80% of the maximum dose value, was 31.1 mm, 29.9 mm, and 30.2 mm for configuration A, B, and C, respectively. The depth dose distributions (experimental and simulated), together with the microdosimetric spectra acquired, are reported in Figures 2, 4 and 6 for configuration A, B, and C, respectively.

The simulated $\bar{L}_t$ and $\bar{L}_d$ (total and primary) and the corresponding experimental

quantities $\bar{y}_F$ and $\bar{y}_D$ obtained from experimental microdosimetry spectra, are shown in Figures 3, 5 and 7 for configuration A, B, and C, respectively. The insets in those figures highlight the compatibility, within the error bars, between Monte Carlo and experimental data, and how the best agreement is given by $\bar{L}_{Total}$, proving the relevance of the secondary ions contribution. The numerical values of $\bar{L}_t$, $\bar{L}_t$, $\bar{y}_F$, and $\bar{y}_D$, for each experimental depth, together with their errors, are all reported in Tables 1, 2 and 3 for configuration A, B, and C, respectively.

The experimental uncertainty on the position where we acquired the microdosimetric spectra was 80 μm for configuration A and B and 150 μm for configuration C. The difference between those two values is due to the different experimental procedures used to evaluate the position. The uncertainty on $\bar{y}_F$ and $\bar{y}_D$ was estimated by applying the error propagation, taking into account the statistical fluctuations of the experimental counts in the microdosimetric spectra and the error on the mean-path length. Due to the experimental uncertainty on the position where the microdosimetric spectra were acquired, each value of $\bar{y}_{F/D}$ has to be compared with a range of Monte Carlo values $\bar{L}_{t/d}$, belonging to that correspondent range of positions. Therefore we assumed, as errors for $\bar{L}_t$ and $\bar{L}_d$, the maximum fluctuation of their value within the interval considered. An additional contribution to the uncertainty on $\bar{L}_t$ and $\bar{L}_d$ for configuration B and C was evaluated: a systematic error, in the order of 5%, due to the modelling of the modulation filters. This contribution has been included since even very tiny inaccuracies in the knowledge of the geometrical and physical characteristics of the modulator can induce relevant differences in the LET output results. The magnitude of the histories in the MC simulations was chosen to have a negligible contribution to the uncertainties given by the statistical fluctuations on $\bar{L}_t$ and $\bar{L}_t$.

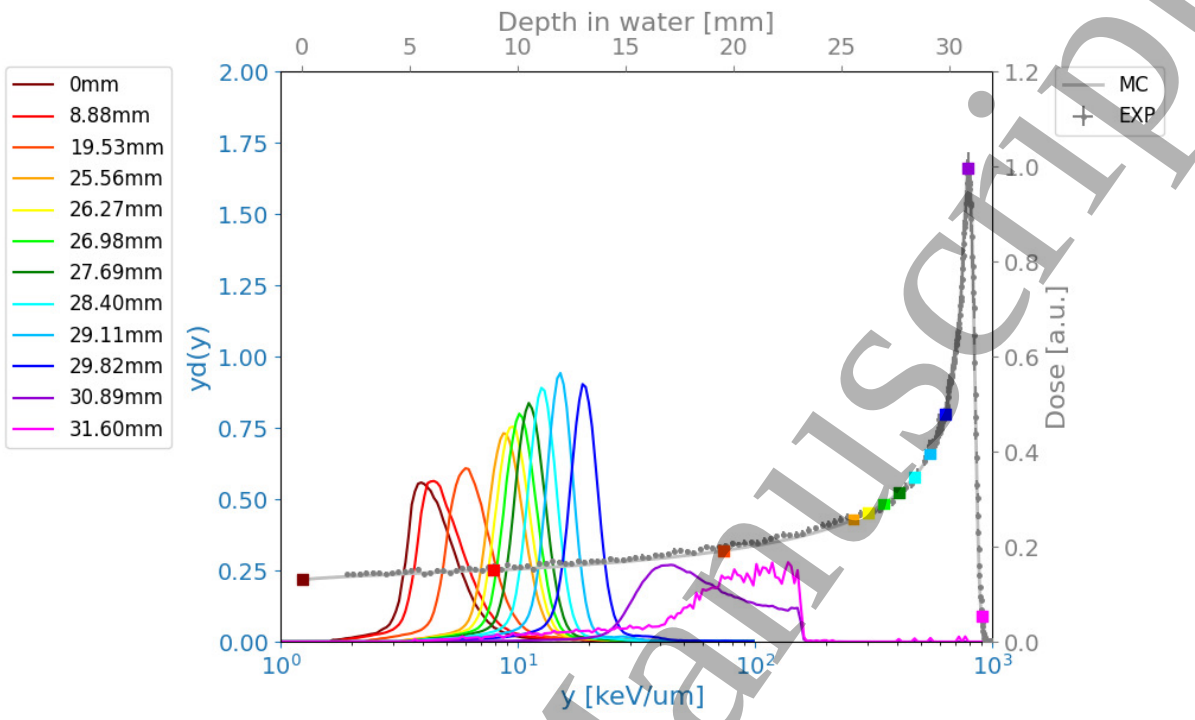

Figure 2. Depth dose profile for configuration A: in dark gray the experimental values obtained with a Markus chamber (mod.3002), in light gray the Geant4 Monte Carlo values. The *yd(y)* microdosimetric distribution measured at twelve different positions between 0 mm (dark red) and 31.60 mm (magenta) are also reported, with the corresponding positions in water depth marked with squares of the corresponding color, along the depth dose profile.

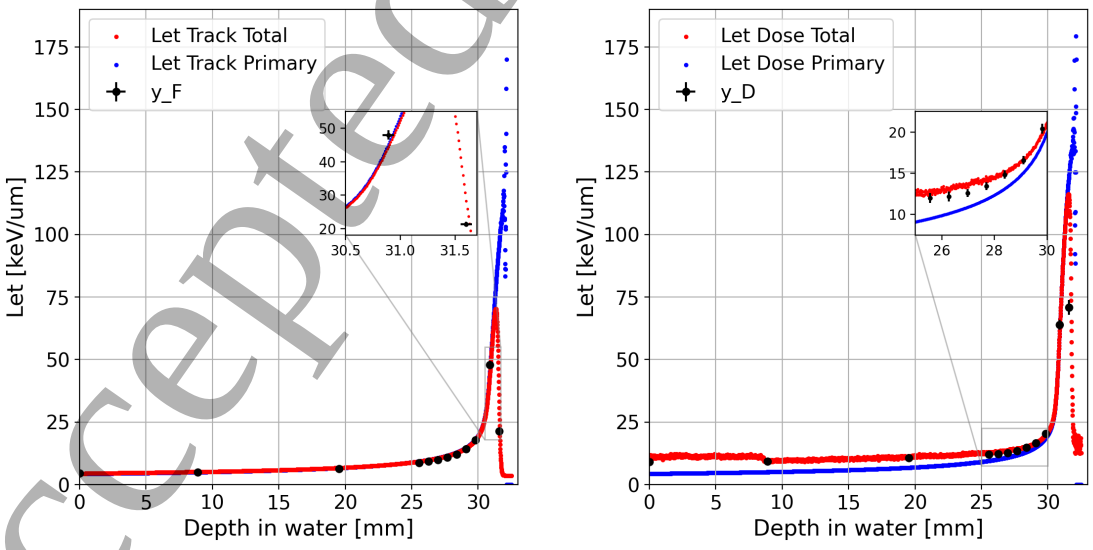

Figure 3. Configuration A: $\bar{y}_F$ values in comparison with the $\bar{L}_t$ values (image on the left), and $\bar{y}_D$ values in comparison with $\bar{L}_d$ values (image on the right): in red $\bar{L}_{t/d}^{Total}$, in blue $\bar{L}_{t/d}$ of the primary, and in black the corresponding microdosimetric quantities $\bar{y}_{F/D}$. The step in the LET total dose curve around 9 mm in water is due to the transition between two different physics models adopted in the simulation for the 4He transport: (the 'ParticleHPInelastic' physics model below 200 AMeV and the 'Binary Light Ion Cascade' above 190 AMeV

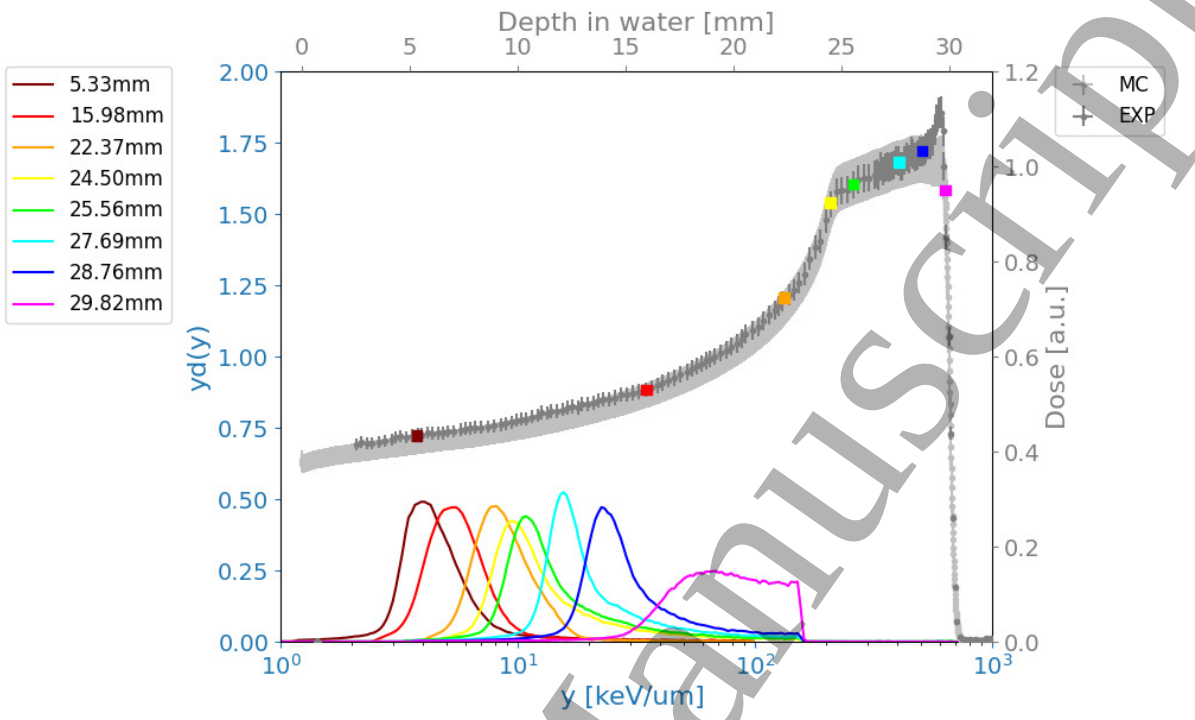

Figure 4. Depth dose profile for configuration B: in dark gray the experimental values obtained with a Markus chamber (mod.3002), in light gray the Geant4 Monte Carlo values. The *yd(y)* microdosimetric distribution measured at eight different positions between 5.33 mm (dark red) and 29.82 mm (magenta) are also reported, with the corresponding positions in water depth marked with squares of the corresponding color, along the depth dose profile.

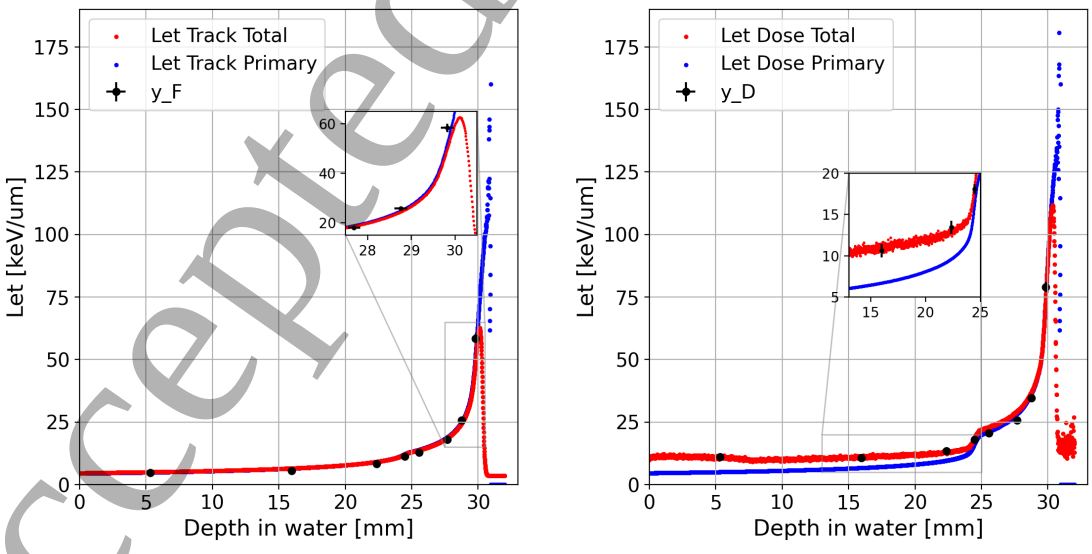

Figure 5. Configuration B: $\bar{y}_F$ values in comparison with the $\bar{L}_t$ values (image on the left), and $\bar{y}_D$ values in comparison with $\bar{L}_d$ values (image on the right): in red $\bar{L}_{t/d}^{Total}$, in blue $\bar{L}_{t/d}$ of the primary, and in black the corresponding microdosimetric quantities $\bar{y}_{F/D}$. The step in the LET total dose curve around 9 mm in water is due to the transition between two different physics models adopted in the simulation for the 4He transport: (the 'ParticleHPInelastic' physics model below 200 AMeV and the 'Binary Light Ion Cascade' above 190 AMeV

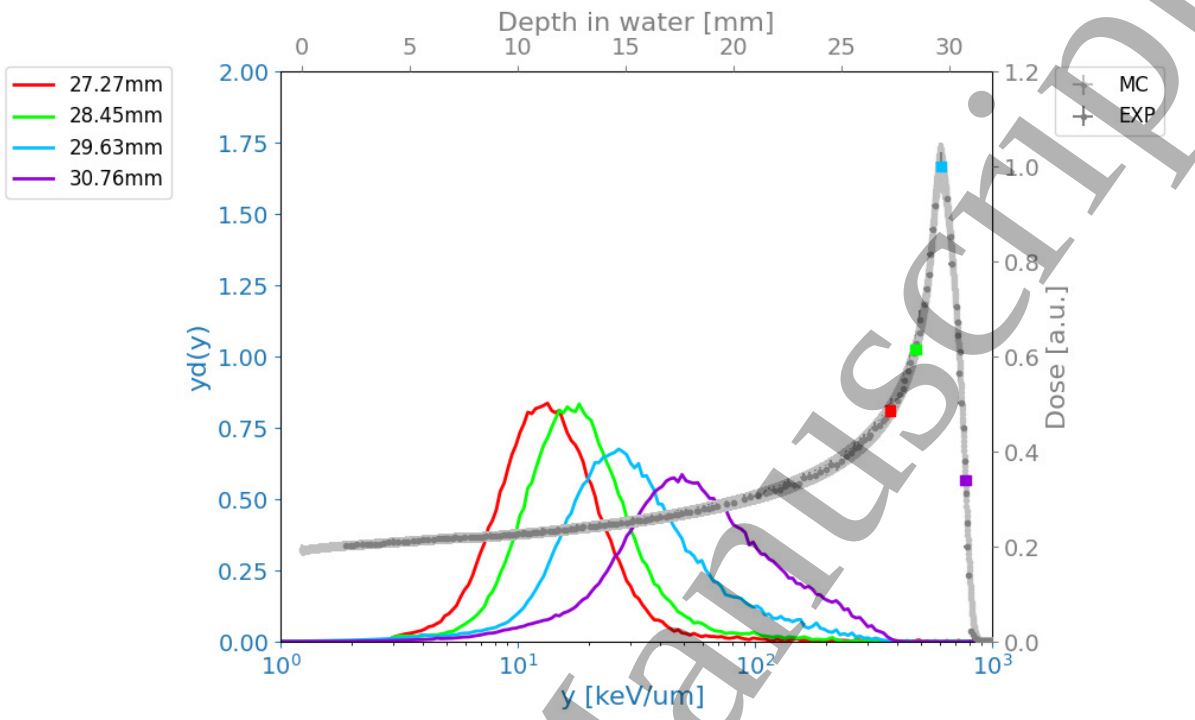

Figure 6. Depth dose profile for configuration C: in dark gray the experimental values obtained with a Markus chamber (mod.3002), in light gray the Geant4 Monte Carlo values. The *yd(y)* microdosimetric distribution measured at four different positions between 27.27 mm (red) and 30.76 mm (violet) are also reported, with the corresponding positions in water depth marked with squares of the corresponding color, along the depth dose profile.

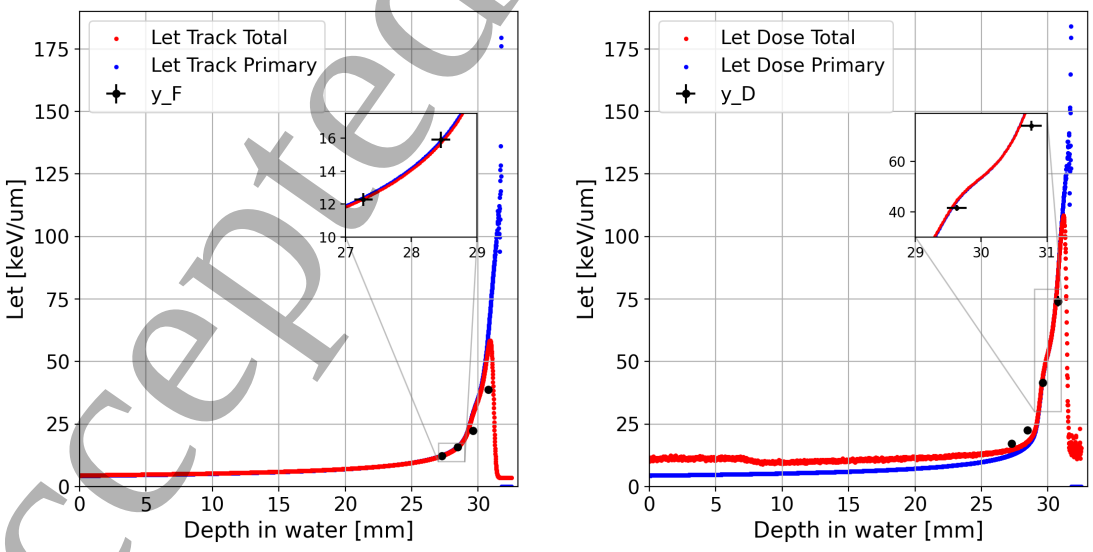

Figure 7. Configuration C: $\bar{y}_F$ values in comparison with the $\bar{L}_t$ values (image on the left), and $\bar{y}_D$ values in comparison with $\bar{L}_d$ values (image on the right): in red $\bar{L}_{t/d}^{Total}$, in blue $\bar{L}_{t/d}$ of the primary, and in black the corresponding microdosimetric quantities $\bar{y}_{F/D}$. The step in the LET total dose curve around 9 mm in water is due to the transition between two different physics models adopted in the simulation for the 4He transport: (the 'ParticleHPInelastic' physics model below 200 AMeV and the 'Binary Light Ion Cascade' above 190 AMeV

Table 1. Configuration A: $\bar{y}_F$ values in comparison with the $\bar{L}_t^{Total}$ values and $\bar{y}_D$ values in comparison with $\bar{L}_d^{Total}$ values.

$depth \pm 0.08$ $[mm]$	$\bar{y}_F \pm \Delta\bar{y}_F$ [keVμm]	$\bar{L}_t^{Total} \pm \Delta\bar{L}_t^{Total}$ [kev/μm]	$\bar{y}_D \pm \Delta\bar{y}_D$ [kev/μm]	$\bar{L}_d^{Total} \pm \Delta\bar{L}_d^{Total}$ [kev/μm]
0.00	4.69 ± 0.14	4.366 ± 0.011	9.2 ± 0.7	9.6 ± 1.0
8.88	5.04 ± 0.15	5.089 ± 0.008	9.6 ± 0.9	9.6 ± 0.7
19.53	6.43 ± 0.19	6.71 ± 0.02	10.9 ± 0.7	11.0 ± 0.5
25.56	8.9 ± 0.3	9.26 ± 0.05	12.2 ± 0.6	12.6 ± 0.5
26.27	9.5 ± 0.3	9.84 ± 0.07	12.4 ± 0.6	13.0 ± 0.3
26.98	10.1 ± 0.3	10.56 ± 0.09	12.8 ± 0.5	13.4 ± 0.4
27.69	11.0 ± 0.3	11.49 ± 0.10	13.7 ± 0.5	14.2 ± 0.5
28.40	12.4 ± 0.4	12.7 ± 0.2	15.1 ± 0.5	14.9 ± 0.4
29.11	14.5 ± 0.4	14.6 ± 0.2	16.9 ± 0.5	16.7 ± 0.3
29.82	18.2 ± 0.5	17.9 ± 0.6	20.8 ± 0.6	19.7 ± 0.8
30.89	48.8 ± 1.4	44 ± 5	65.0 ± 1.9	61 ± 9
31.60	21.7 ± 0.7	30 ± 20	72 ± 3	114 ± 13

Table 2. Configuration B: $\bar{y}_F$ values in comparison with the $\bar{L}_t^{Total}$ values and $\bar{y}_D$ values in comparison with $\bar{L}_d^{Total}$ values.

$depth \pm 0.08$ $[mm]$	$\bar{y}_F \pm \Delta\bar{y}_F$ [keVμm]	$\bar{L}_t^{Total} \pm \Delta\bar{L}_t^{Total}$ [kev/μm]	$\bar{y}_D \pm \Delta\bar{y}_D$ [kev/μm]	$\bar{L}_d^{Total} \pm \Delta\bar{L}_d^{Total}$ [kev/μm]
5.33	4.89 ± 0.14	5.1 ± 0.3	11.3 ± 0.8	11.2 ± 0.7
15.98	5.73 ± 0.17	6.5 ± 0.3	9.8 ± 0.8	11.4 ± 1.3
22.37	8.5 ± 0.3	9.1 ± 0.5	13.7 ± 0.8	13.2 ± 1.5
24.50	11.5 ± 0.3	12.1 ± 0.8	18.4 ± 0.6	19 ± 2
25.56	13.1 ± 0.4	13.8 ± 0.8	20.8 ± 0.7	23.1 ± 1.7
27.69	18.3 ± 0.5	18.6 ± 1.2	26.1 ± 0.8	29 ± 2
28.78	26.2 ± 0.8	24.4 ± 1.8	35.2 ± 1.0	37 ± 3
29.82	$59.4 \pm \pm 1.7$	50 ± 7	80 ± 2	73 ± 12

Table 3. Configuration C: $\bar{y}_F$ values in comparison with the $\bar{L}_t^{Total}$ values and $\bar{y}_D$ values in comparison with $\bar{L}_d^{Total}$ values.

$depth \pm 0.15$ $[mm]$	$\bar{y}_F \pm \Delta\bar{y}_F$ [keVμm]	$\bar{L}_t^{Total} \pm \Delta\bar{L}_t^{Total}$ [kev/μm]	$\bar{y}_D \pm \Delta\bar{y}_D$ [kev/μm]	$\bar{L}_d^{Total} \pm \Delta\bar{L}_d^{Total}$ [kev/μm]
27.27	12.3 ± 0.3	12.3 ± 0.8	17.3 ± 1.2	14.7 ± 1.3
28.45	15.9 ± 0.2	15.7 ± 1.3	22.7 ± 0.7	18.1 ± 1.5
29.63	22.4 ± 0.2	29 ± 4	41.5 ± 1.0	45 ± 7
30.76	38.9 ± 0.4	56 ± 7	74 ± 2	85 ± 13

3.2. Statistical Test

The agreement between the simulation and experimental data was evaluated by performing the χ^2 Test.

For the goodness of fit test, we established the null hypothesis H_0 that the experimental data fits the expected data given by the Monte Carlo; the level of significance chosen was $\alpha = 0.05$. Then we proceed with the χ^2 Test comparing $\bar{L}_t$ with $\bar{y}_F$: (Taylor 1997)

$$\chi^2_{LET_T - Y_F} = \sum \frac{(LET_T - Y_F)^2}{(\sigma^2_{LET_T} + \sigma^2_{Y_F})} \tag{9}$$

and similarly for $\bar{L}_d$ with $\bar{y}_D$.

Table 4 reports the results of the χ^2 test as well as the number of degrees of freedom (DoF) and the critical value (C.V.) for each configuration.

Table 4. Results of the χ^2 test for the three configurations at the level of significance established of $\alpha = 0.05$.

	Configuration		
	A DoF = 12 C.V. = **21.0**	**B** DoF = 8 C.V. = **15.5**	**C** DoF = 4 C.V. = **9.49**
$\chi^2_{\bar{y}_T - \bar{L}_T^{Total}}$	**16.5** (p-value = 0.169)	**9.57** (p-value = 0.297)	**9.32** (p-value = 0.054)
$\chi^2_{\bar{y}_D - \bar{L}_D^{Total}}$	**14.8** (p-value = 0.253)	**6.09** (p-value = 0.637)	**9.21** (p-value = 0.056)

From Table 4, we can see that, for all the configurations, the χ^2 result is below the C.V. both for $\bar{y}_F$ compared to $\bar{L}_t^{Total}$ and $\bar{y}_D$ to $\bar{L}_d^{Total}$ and consequently all the p-values are greater than α. So we can conclude that all the χ^2 Test results fall into the acceptance region (area below the C.V.), and, in all cases, the null hypothesis H_0 that the experimental data fit the expected data given by Monte Carlo, can be accepted.

3.3. Study of the LET values due to the single secondary ions

It is interesting to investigate the contribution of secondary ions, produced along the depth, on the LET. For this purpose specific Monte Carlo simulations were realized, enabling the Let algorithms to record the values upon the condition of having the energy deposit by a particle with a given atomic number. The results of these Monte Carlo simulations are presented in Figure 8, Figure 9 and Figure 10 for configurations A, B, and C, respectively. To understand the possible biological consequences of those particles' contributions, regardless of their low fluxes (see Figure 11), we explored the available data of RBE vs LET (McNamara *et al.* 2015, Sørensen *et al.* 2011, Friedrich *et al.* 2017).

In McNamara *et al.* (2015) is shown as an increasing LET ($\bar{L}_d$) implies increasing RBE values. However, their phenomenological RBE model is derived from proton experimental data with $\bar{L}_d$ up to 20 keV/μm. In the review of Sørensen *et al.* (2011) an ensemble of more than 200 RBE values, three different cell lines and different ion species are presented. With those data they show how RBE increases with LET increase, up to a maximum for LET values

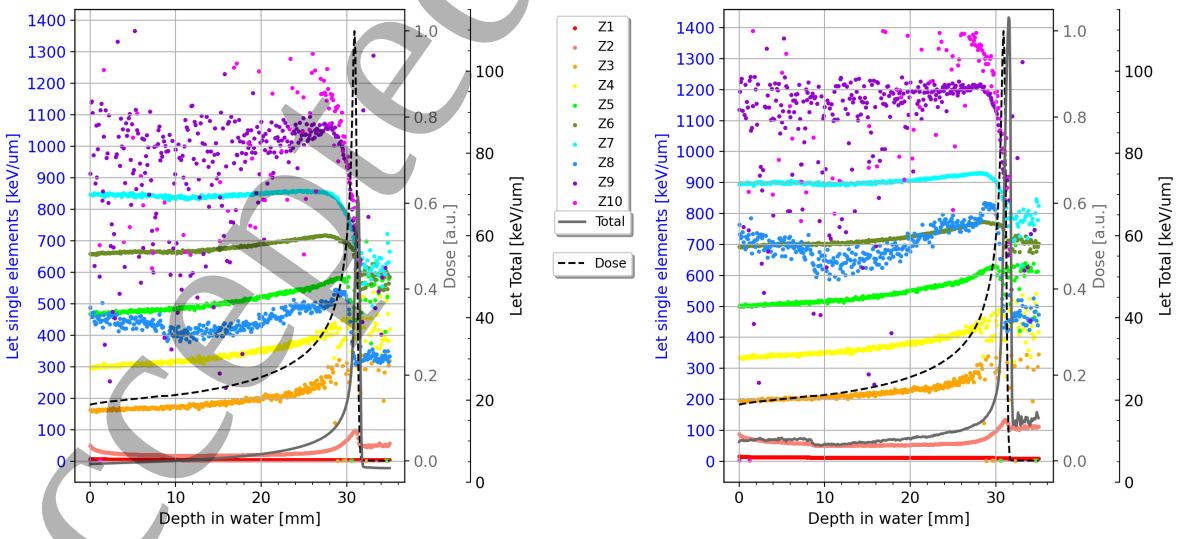

Figure 8. Configuration A: contribution to $\bar{L}_t^{Total}$ (on the left), and on $\bar{L}_d^{Total}$ (on the right), due to the single secondary ions from Z=1 (red) to Z=10 (magenta). In gray (solid line) we have $\bar{L}_{t/d}^{Total}$ and in gray (dashed line) the dose profile, both with their own axis scale, on the right side of each picture.

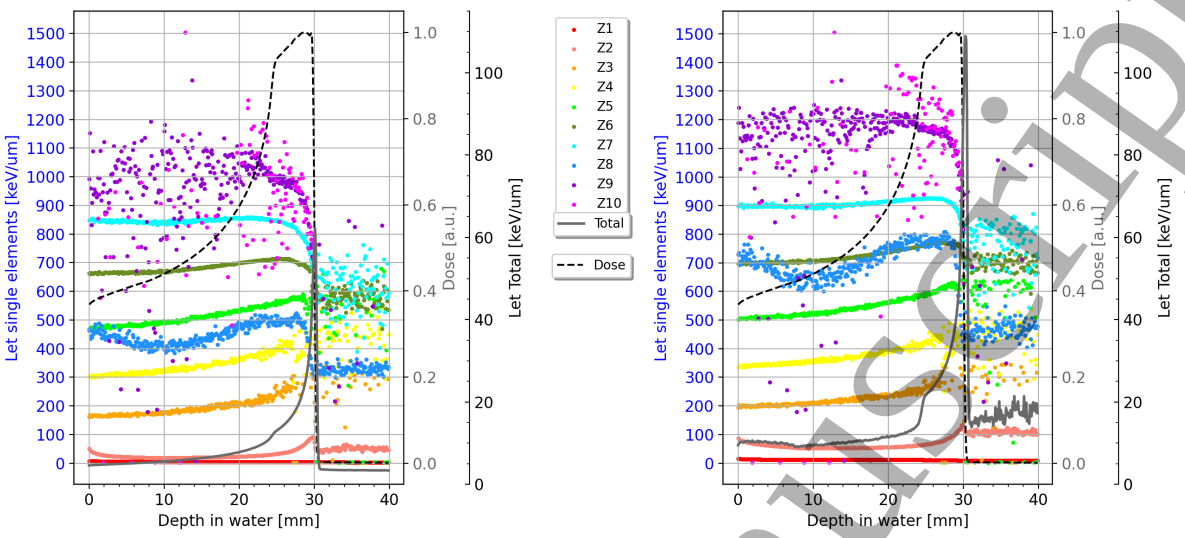

Figure 9. Configuration B: contribution to $\bar{L}_t^{Total}$ (on the left), and on $\bar{L}_d^{Total}$ (on the right), due to the single secondary ions from Z=1 (red) to Z=10 (magenta). In gray (solid line) we have $\bar{L}_{t/d}^{Total}$ and in gray (dashed line) the dose profile, both with their own axis scale, on the right side of each picture.

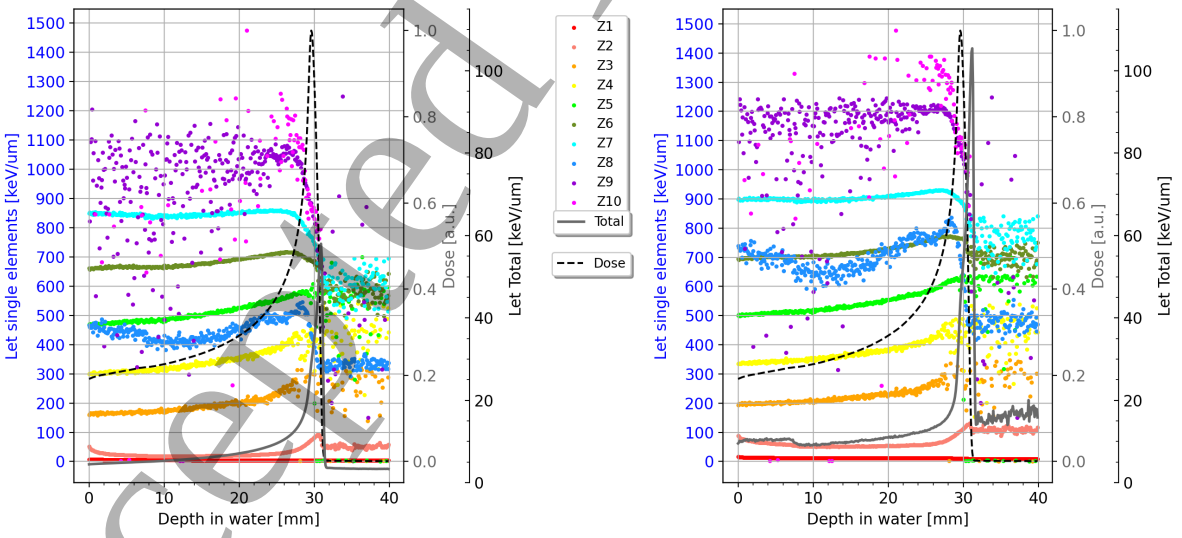

Figure 10. Configuration C: contribution to $\bar{L}_t^{Total}$ (on the left), and on $\bar{L}_d^{Total}$ (on the right), due to the single secondary ions from Z=1 (red) to Z=10 (magenta). In gray (solid line) we have $\bar{L}_{t/d}^{Total}$ and in gray (dashed line) the dose profile, both with their own axis scale, on the right side of each picture.

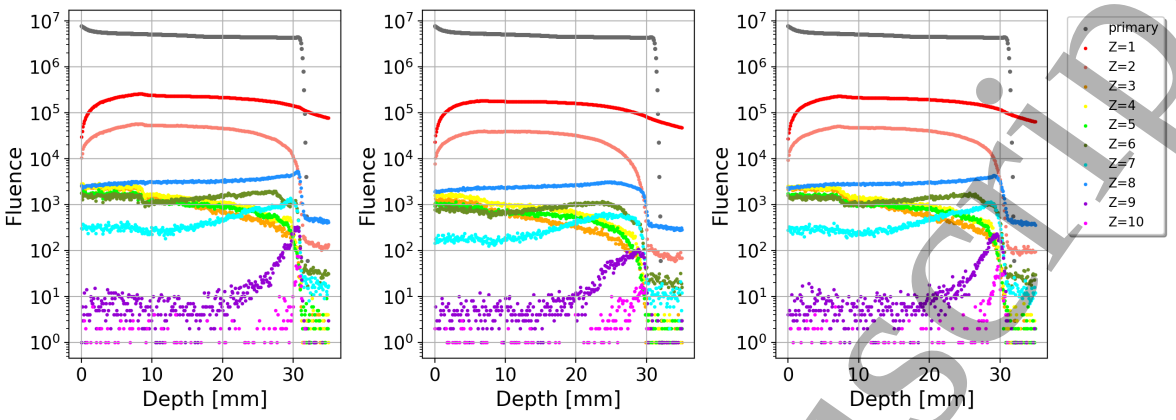

Figure 11. Fluences of secondary ions from Z=1 (red) to Z=10 (magenta), against 10^7 primaries (gray), obtained with Monte Carlo simulations: from left to right configuration A, B and C respectively.

of 100-200 keV/μm, and then decreases for further LET increase. This RBE vs LET trend was confirmed in the very recent PIDE (Particle Irradiation Data Ensemble) publication (Friedrich *et al.* 2017), as well.

In Figure 12, we show the plots obtained with the data from Sørensen *et al.* (2011) review, selecting the ions relevant for our study: on the left there are all RBE vs LET data, in the middle the RBE vs $\bar{L}_t$, and in the right RBE vs $\bar{L}_t$. As shown in Figure 12, all RBE-LET data points show a high level of agreement with each other among the different ion species. From an inspection of the plots in Figure 12, we can define different "RBE Levels" ($RBE_{threshold}$),

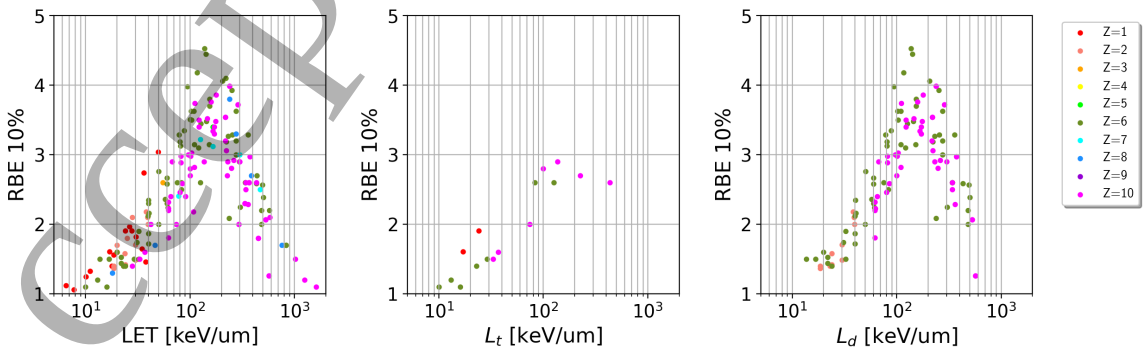

Figure 12. RBE vs LET for different ions from Z=1 (red) to Z=10 (magenta): from left to right RBE vs all LET values, Lt and Ld respectively (Sørensen *et al.* 2011).

based on specific thresholds, and we can determine, for each of them, the corresponding range of LET values:

- $RBE_{4.0}$ (RBE $>$ 4.0): LET in the range 100 - 200 keV/μm
- $RBE_{3.5}$ (RBE $>$ 3.5): LET in the range 100 - 300 keV/μm
- $RBE_{3.0}$ (RBE $>$ 3.0): LET in the range 75 - 300 keV/μm
- $RBE_{2.5}$ (RBE $>$ 2.5): LET in the range 50 - 500 keV/μm
- $RBE_{2.0}$ (RBE $>$ 2.0): LET in the range 25 - 600 keV/μm

From a qualitative analysis of our plots of single ions LET, it is possible to identify the fragments giving a significant contribution, in the entrance or the distal region of the SOBP, to each of the RBE levels above defined. The results obtained are presented in Table 5. Results are in agreement with those presented by Burigo (Burigo *et al.* 2014) .

Table 5. Analysis of the single fragments $\bar{L}_d$ and $\bar{L}_t$ to identify their RBE level at the entrance and in the distal part of all the Bragg peak distributions. Unless otherwise specified, it is considered valid for all three configurations studied.

RBE Level	LET	Z Value of Fragments	
		Entrance	Distal
4.0	Dose	3	2
3.5	Dose	3	2, 3 (configuration B and C)
3.0	Dose	3	2, 3 (configuration B and C)
2.5	Dose	2, 3, 4	2, 3, 4, 8
	Track	3, 4, 5, 8	2, 3, 4, 8
2.0	Dose	2, 3, 4, 5	2, 3, 4, 8

As shown in Table 5, $RBE_{4.0}$, $RBE_{3.5}$, and $RBE_{3.0}$ get contributions only from Lithium in the entrance and secondary Helium, plus Lithium for the modulated configurations, in the distal. All other fragments, with Z between 4 and 8, contribute to lower RBE values. Fragments with Z equal to 9 and 10, besides having a subdominant relative fluence, do not participate in any of the RBE levels defined, since their LET values are mainly ranging between 700 and 1500 keV/μm.

For $RBE_{2.5}$, both dose and track averaged LET distributions were analyzed. As shown in Table 5, results are consistent in the distal part while there are some differences in the entrance. Anyway, this is quite reasonable since the RBE vs $\bar{L}_d^{Total}$ study is not supported yet with adequate data contributions, so it is more difficult to draw reliable conclusions.

From the above considerations we can conclude that ions with very high LET (1000-1500 keV/μm), which can be stoppers in sensitive volumes, are not producing essential change in a final RBE determination with depth, in ^{4}He therapy. This explains the agreement in RBE derived by MicroPlus probe and nano-TEPC (Conte *et al.* 2020).

4. Discussion and conclusions

A very appealing candidate for the realization of brand new treatment plans, both mono and multi-ion type, is ^{4}He, also considering the very successful trial carried out in the years 1977-1993 at LBNL. Moreover, nowadays, ^{4}He has come back in the spotlight thanks to the ongoing clinical translation at the Heidelberg Ion-Beam Therapy Center (Mein *et al.* 2019, Ebner *et al.* 2017).

This work has aimed to extend the study and the understanding of biological-relevant quantities for the case of ^{4}He ion.

The calculation of total averaged-LET quantities, through Monte Carlo based algorithms (Petringa *et al.* 2020), was extended to the ^{4}He ion that, besides the target fragmentation, shows a relevant contribution due to the projectile fragmentation.

The Let algorithms were validated by comparing their output with experimental data obtained using two different microdosimeters and adopting three different irradiation set-ups. As shown in the results presented in Section 3, and verified with the statistical analysis based on the χ^2 goodness of fit test, the total averaged LET quantities obtained with the Monte Carlo calculations, including all the contributions of secondary ions, find a remarkable agreement

with the microdosimetric experimental data, within their respective uncertainties, that also justified application of MicroPlus and nano-TEPC microdosimeters in particle therapy in clinical settings. Good agreement of $\bar{L}_d^{Total}$ with $\bar{y}_D$ experimentally measured with, in a plato region where high LET secondaries contribute, essentially confirmed that MicroPlus measures adequately direct and secondary ions. This is supported by the recently published application of MicroPlus for RBE and cell survival fraction verification in ^{4}He ion beam with energy up to 166 MeV/u (Lee *et al.* 2021).

The results of this study certify the use of a very effective tool for the precise calculation of LET, given by a Monte Carlo approach which has the advantage of allowing detailed simulation and tracking of nuclear interactions, even in complex clinical scenarios. Furthermore, this tool does not fear the limitation due to the usual high CPU consumption time, typical of this approach. One can limit the CPU-time by setting high cuts in the production of secondary particles without losing accuracy in the results, as it was verified and demonstrated in Petringa *et al.* (2020). In this study, using a cut of 10 μm, a statistically significant run could be accomplished in less than 8 hours with ten threads in parallel on a processor with a 3.2 GHz CPU.

At last, a study to investigate the contribution of secondary ions on the LET, was realized with dedicated Monte Carlo simulations. Out of this study a discussion on the biological role of secondary ions was done referring to the existing literature of RBE data vs LET.

Acknowledgment

This work was supported by the National Institute for Nuclear Physics (INFN) that funded the MoVeIT and NEPTUNE project. Moreover it was performed in the framework of the MC-INFN (Monte Carlo at INFN) initiative also funded by the Interdisciplinary Committee of INFN. A. Ristić-Fira and I. Petrović wish to acknowledge financial support from INFN

Fondo Affari Internazionali (FAI), MAECI PGR No. 00794 Italy - Serbia Project, as well as European Union HORIZIN2020 research and innovation program (Grant Agreement n 654002 ENSAR2) and from the Ministry of Education, Science and Technological Development of Serbia.

References

Agostinelli, S. *et al.* (2003). Geant4 - a simulation toolkit, *Nuclear Instruments and Methods in Physics Research A* **506**: 250–303.
URL: *https://doi.org/10.1016/S0168-9002(03)01368-8*

Allison, J., Amako, K., Apostolakis, J. *et al.* (2006). Geant4 developments and applications, *IEEE Transactions on Nuclear Science* **53**: 270–278.
URL: *https://doi.org/10.1109/TNS.2006.869826*

Allison, J., Amako, K., Apostolakis, J. *et al.* (2016). Recent developments in GEANT4, *Nuclear Instruments and Methods in Physics Research A* **835**: 186-225.
URL: *https://doi.org/10.1016/j.nima.2016.06.125*

Anderson, S. & other (2017). Microdosimetric measurements of a clinical proton beam with micrometer-sized solid-state detector, *Medical Physics* **44(11)**: 6029-6037.
URL: *https://doi.org/10.1002/mp.12583*

Bertolet, A. *et al.* (2019). Dose-averaged LET calculation for proton track segments using microdosimetric monte carlo simulations, *Medical Physics* **46(9)**: 4184-4192.
URL: *https://doi.org/10.1002/mp.13643*

Bolst, D. *et al.* (2017). Correction factors to convert micro- dosimetry measurements in silicon to tissue in ^{12}C ion therapy, *Physics in Medicine and Biology* **62**: 2055-2069.
URL: *http://dx.doi.org/10.1088/1361-6560/aa5de5*

Bortot, D. *et al.* (2017). A novel avalanche-confinement TEPC for microdosimetry at nanometric level, *Radiation Measurements* **103**: 1-12.
URL: *https://www.sciencedirect.com/science/article/pii/S1350448717300690*

Bourhaleb, F. *et al.* (2017). Monte Carlo simulations of ripple filters designed for proton and carbon ion beams in hadrontherapy with active scanning technique, *Journal of Physics: Conference Series* **102**: 012002.
URL: *http://dx.doi.org/10.1088/1742-6596/102/1/012002*

Cirrone, G. *et al.* (2005). Implementation of a new Monte Carlo-GEANT4 Simulation tool for the development of a proton therapy beam line and verification of the related dose distributions, *IEEE Transaction Nuclear Science* **52**: 262-265.

URL: *https://doi.org/10.1109/TNS.2004.843140*

Cirrone, G. *et al.* (2011). Hadrontherapy: a Geant4-Based Tool for Proton/Ion-Therapy Studies, *Progress in Nuclear Science Technology* **2**: 207-212.

URL: *https://doi.org/10.15669/pnst.2.207*

Cirrone, G. *et al.* (2017). Clinical and Research Activities at the CATANA Facility of INFN-LNS: From the Conventional Hadrontherapy to the Laser-Driven Approach, *Frontiers in Oncology* **7**: 223.

URL: *https://doi.org/10.3389/fonc.2017.00223*

Conte, V. *et al.* (2020). Microdosimetry of a therapeutic proton beam with a mini-TEPC and a MicroPlus-Bridge detector for RBE assessment, *Physics in Medicine and Biology* **65(24)**: 245018.

URL: *https://iopscience.iop.org/article/10.1088/1361-6560/abc368*

Cortes-Giraldo, M. & Carabe, A. (2015). A critical study of different Monte Carlo scoring methods of dose average linear-energy-transfer maps calculated in voxelized geometries irradiated with clinical proton beams, *Physics in Medicine and Biology* **60**: 2645-2669.

URL: *https://iopscience.iop.org/article/10.1088/0031-9155/60/7/2645*

Ebner, D. K. *et al.* (2021). The Emerging Potential of Multi-Ion Radiotherapy, *Frontiers in Oncology* **11**: 624786.

URL: *https://www.frontiersin.org/article/10.3389/fonc.2021.624786*

Friedrich, T., Pfuhl, T. & Scholz, M. (2021). Update of the particle irradiation data ensemble (PIDE) for cell survival, *Journal of Radiation Research* **62-4**: 645-655.

URL: *https://doi.org/10.1093/jrr/rrab034*

Geant4 Physics List Guide (2020).

URL: *https://geant4-userdoc.web.cern.ch/UsersGuides/PhysicsListGuide*

Geant4 Physics Reference Manual (2020).

URL: *https://geant4-userdoc.web.cern.ch/UsersGuides/PhysicsReferenceManual*

Hawkins, R. B. (2003). A Microdosimetric-Kinetic Model for the Effect of Non-Poisson Distribution of Lethal Lesions on the Variation of RBE with LET, *Radiation Research* **160**: 61-69.

URL: *https://doi.org/10.1667/RR3010*

International Commission on Radiation Units & Measurements (eds) (1983). *ICRU Report No 36, Microdosimetry*, Bethesda, MD: International Commission on Radiation Units and Measurements.

URL: *https://doi.org/10.1093/jicru/os19.1.Report36*

Ivanchenko, V. *et al.* (2014). Geant4 electromagnetic physics: improving simulation performance and accuracy, *International Conference on Supercomputing in Nuclear Applications and Monte Carlo*.

URL: *https://doi.org/10.1051/snamc/201403101*

Kalholm, F. *et al.* (2021). A systematic review on the usage of averaged LET in radiation biology for particle therapy, *Radiotherapy and Oncology*. **161**: 211-221.

URL: *https://doi.org/10.1016/j.radonc.2021.04.007*

Kantemiris, I. *et al.* (2011). Dose and dose averaged LET comparison of ^1H, ^4He, ^6Li, ^8Be, ^{10}B, ^{12}C, ^{14}N, and ^{16}O ion beams forming a spread-out Bragg peak, *Medical Physics* **38**: 6585-6591.

URL: *https://doi.org/10.1118/1.3662911*

Krämer, M. *et al.* (2016). Helium ions for radiotherapy? Physical and biological verifications of a novel treatment modality, *Medical Physics* **43-4**: 1995-2004.

URL: *https://doi.org/10.1118/1.4944593*

Kurz, C., Mairani, A. & Parodi, K. (2012). First experimental-based characterization of oxygen ion beam depth dose distributions at the Heidelberg Ion-Beam Therapy Center, *Physics in Medicine and Biology* **57**: 5017.

URL: *https://doi.org/10.1088/0031-9155/57/15/5017*

Lee, S. H. *et al.* (2021). Estimating the biological effects of helium, carbon, oxygen, and neon ion beams using 3D silicon microdosimeters, *Physics in Medicine and Biology* **66**: 045017.

URL: *https://iopscience.iop.org/article/10.1088/1361-6560/abd66f*

Mairani, A. *et al.* (2021). FLASH Dose-Rate Helium Ion Beams: First In Vitro Investigations, *International Journal of Radiation Oncology, Biology, Physics* **111-3**: S20-S21.

URL: *https://doi.org/10.1016/j.ijrobp.2021.07.076*

Malouff, T. D. *et al.* (2020). Carbon Ion Therapy: A Modern Review of an Emerging Technology, *Frontiers in Oncology* **10**: 82.

URL: *https://doi.org/10.3389/fonc.2020.00082*

Mazzucconi, D. *et al. (a)* (2018). MICRODOSIMETRY AT NANOMETRIC SCALE WITH AN AVALANCHE-CONFINEMENT TEPC: RESPONSE AGAINST A HELIUM ION BEAM, *Radiation Protection Dosimetry* **183-1-2**: 177-181.

URL: *https://doi.org/10.1093/rpd/ncy230*

Mazzucconi, D. *et al. (b)* (2018). Monte Carlo simulation of a new TEPC for microdosimetry at nanometric

level: Response against a carbon ion beam, *Radiation Measurements* **113**: 7-13.

URL: *https://doi.org/10.1016/j.radmeas.2018.03.006*

McNamara, A. L., Schuemann, J. & Paganetti, H. (2015). A phenomenological relative biological effectiveness (RBE) model for proton therapy based on all published in vitro cell survival data, *Physics in Medicine and Biology* **60**: 8399-8416.

URL: *https://iopscience.iop.org/article/10.1088/0031-9155/60/21/8399*

Mein, S. *et al.* (2019). Biophysical modeling and experimental validation of relative biological effectiveness (RBE) for ^4He ion beam therapy, *Radiation Oncology* **14**: 123.

URL: *https://doi.org/10.1186/s13014-019-1295-z*

Norbury, J. W. *et al.* (2020). Are Further Cross Section Measurements Necessary for Space Radiation Protection or Ion Therapy Applications? Helium Projectiles, *Frontiers in Physics* **8**: 409.

URL: *https://doi.org/10.3389/fphy.2020.565954*

Petringa, G. *et al.* (2020). Monte Carlo implementation of new algorithms for the evaluation of averaged-dose and -track linear energy transfers in 62 MeV clinical proton beams, *Physics in Medicine and Biology* **65**: 235043.

URL: *https://iopscience.iop.org/article/10.1088/1361-6560/abaeb9*

Romano, F. *et al.* (2014). A Monte Carlo study for the calculation of the average linear energy transfer (LET) distributions for a clinical proton beam line and a radiobiological carbon ion beam line, *Physics in Medicine and Biology* **59(12)**: 2863-8.

URL: *https://iopscience.iop.org/article/10.1088/0031-9155/59/12/2863*

Rosenfeld, A. (2016). Novel detectors for silicon based microdosimetry, their concepts and applications, *Nuclear Instruments and Methods in Physics Research Section A* **809**: 156-170.

URL: *http://dx.doi.org/10.1016/j.nima.2015.08.059*

Sokol, O. *et al.* (2017). Oxygen beams for therapy: advanced biological treatment planning and experimental verification, *Physics in Medicine and Biology* **62**: 7798.

URL: *https://iopscience.iop.org/article/10.1088/1361-6560/aa88a0*

Sørensen, B. S., Overgaard, J. & Bassler, N. (2019). In vitro RBE-LET dependence for multiple particle types, *Acta Oncologica* **50:6**: 757-762.

URL: *http://dx.doi.org/10.3109/0284186X.2011.582518*

Taylor, J. R. (1997). *An Introduction to Error Analysis: The Study of Uncertainties in Physical Measurement - Second Edition*, Univ Science Books (ed.) ISBN 10: 093570275X ISBN 13: 9780935702750

Tsujii, H. & Kamada, T. (2012). A Review of Update Clinical Results of Carbon Ion Radiotherapy, *Japanese Journal of Clinical Oncology* **42-8**: 670-685.

URL: *https://doi.org/10.1093/jjco/hys104*

Tessonnier, T. *et al.* (2017). Dosimetric verification in water of a Monte Carlo treatment planning tool for proton, helium, carbon and oxygen ion beams at the Heidelberg Ion Beam Therapy Center, *Physics in Medicine and Biology* **62**: 6579.

URL: *https://iopscience.iop.org/article/10.1088/1361-6560/aa7be4*

Tessonnier, T. *et al.* (2021). Next Evolutions in Particle Therapy: Helium Ion Treatment Planning, Delivery and Clinical Implications of Biological Modeling, *International Journal of Radiation Oncology Biology Physics* **111-3**: e516-e517.

URL: *https://doi.org/10.1016/j.ijrobp.2021.07.1414*

Tommasino, F. & Durante, M. (2015) Proton Radiobiology, *Cancers* **7**: 353-381.

URL: *https://doi.org/10.3390/cancers7010353*

Weber, U. & Kraft, G. (1999) Design and construction of a ripple filter for a smoothed depth dose distribution in conformal particle therapy, *Physics in Medicine and Biology* **44**: 2765.

URL: *https://doi.org/10.1088/0031-9155/44/11/306*

Wilkens, J. & Oelfke, U. (2003). Analytical linear energy transfer calculations for proton therapy, *Medical Physics* **30**: 806-815. **URL:** *https://doi.org/10.1118/1.1567852*

Carante, M.P. *et al.* (2018). BIANCA, a biophysical model of cell survival and chromosome damage by protons, C-ions and He-ions at energies and doses used in hadrontherapy, *Physics in Medicine and Biology* **63**: 75007.

URL: *https://iopscience.iop.org/article/10.1088/1361-6560/aab45f*

Burg, L. *et al.* (2014). Microdosimetry spectra and RBE of 1H, 4He, 7Li and 12C nuclei in water studied with Geant4, *Nuclear Instruments and Methods B* **320**: 89.

URL: *https://doi.org/10.1016/j.nimb.2013.10.018*